# Compression performance of ultra-high performance concrete filled steel tube(UHPCFST) columns exposed to elevated temperature during construction

Tan Wang[a], Min Yu[a]*, Wenlan Liao[a], Chunlei Yu[a], Jianqiao Ye[b]

[a] School of Civil Engineering, Wuhan University, Wuhan 430072, China;

[b] School of Engineering, Lancaster University, Lancaster LA1 4YR, UK

**Abstract:** To investigate the residual mechanical performance of ultra-high performance concrete filled steel tube (UHPCFST) columns exposed to high temperatures during construction, in this research, an experimental study on 27 UHPCFST columns is conducted to examine the impact of fire scenarios, age of the core UHPC exposed to elevated temperature, and volume ratio of coarse aggregates on the post fire behavior of the UHPCFST columns. Detailed analyses are carried out on the failure modes, the historical maximum temperatures in the cross-sections, the axial load-deformation curve, the residual compressive strengths, and the residual stiffness of the columns. The findings indicate that both the steel tubes and the bearing capacity UHPC cores show increases in the historical maximum temperatures with the increase in the aging of the core UHPC. For columns exposed to fire sources at greater distances, a significant enhancement in bearing capacity was observed following high-temperature exposure at varying ages. The bearing capacity demonstrated an increasing trend with the aging of the UHPC subjected to high temperatures. In contrast, when exposed to nearby fire sources, a decline in strength was noted, and the overall bearing capacity of the columns decreased as the age of UHPC exposed to elevated temperature increased. Furthermore, a predictive model for the residual bearing capacity of UHPCFST columns subjected to high temperatures during construction was developed and validated. This research is expected to provide valuable insights for the post-fire evaluation and reinforcement of UHPCFST structure in construction settings.

**Keywords:** Ultra-high-performance concrete-filled steel tube; Post fire; Early-age UHPC; During construction; Residual bearing capacity.

## 1 Introduction

Ultra-high performance concrete (UHPC) is a high-strength, high-toughness, low-porosity advanced cementitious material. The application of UHPC structures can significantly reduce the volume of concrete required in building structures and extend their service life, aligning with the current demand for full lifecycle usage in construction[1, 2]. However, UHPC has issues such as susceptibility to explosive spalling under high temperatures[3-6] and limited ductility[7-10]. Encasing UHPC in steel tubes to create UHPC filled steel tube columns (UHPCFST) not only effectively prevents explosive spalling[11] at high temperatures but also enhances the overall ductility of the structure[12-15], and it is expected to gain increasing favor in practical engineering.

Furthermore, fire is one of the most common accidental disasters that building structures are vulnerable to. Therefore, fire-resistant design has become a crucial component in the lifecycle design of engineering structures. The fire resistance and post-high temperature residual performance of UHPCSFT components form the foundation of fire-resistant design for such structures. To understand the current state of research in this field, several key studies are noteworthy. For example, Xiong[16] investigates the structural fire performance of ultra-high-strength concrete filled steel tubular (CFST) columns, and found that the CFST columns with ultra-high-strength concrete exhibited similar fire performance to those with normal/high strength concrete with respect to thermal expansion, axial contraction and failure modes; Yao[17] studied the axial compression performance of UHPCFCST stub columns after exposure to high temperatures and revealed that the restraining effect of the steel tube prevented the core UHPC from bursting at high temperatures. The temperature field[18], fire resistance[19] and post-fire performance[20] of UHPCFST columns were invested systematically also in the author's previous work.The above investigations have piloted the research on fire resistance of the UHPCFST.

The safety and reliability of an engineering structure during the construction phase are vital components of the lifecycle risk analysis and control of the structure. Statistics has indicated that accidents during the construction phase are significantly more frequent than in the normal service phase[21]. Incidents of fire during construction or renovation stages are frequently reported in the media almost every year[22-24], as exampled in Figure 1, often associated with extensive welding, cutting, and temporary electrical usage[25, 26]. The mechanisms of high-temperature degradation and fire resistance of building structures during construction are notably different from those in the service phase, mainly due to: 1) The steel

structures typically lack effective fire protection during construction, making them highly susceptible to instability and failure under fire; 2) Some concrete structures are younger than 28 days, with hydration not yet complete. Their performance at high temperatures and the development of fire damage over time differ significantly from that of fully hardened concrete[27]. Therefore, it is necessary to conduct research on the fire resistance of engineering structures considering the impact of fires during the construction phase.

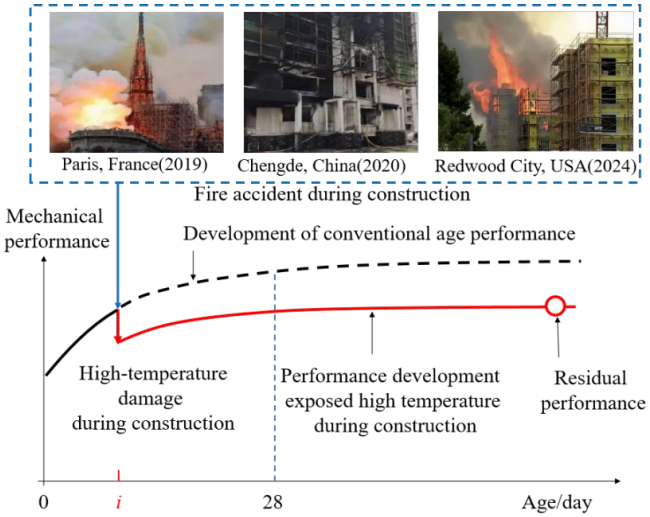


Figure 1 Fire accidents and damage during construction

After a fire, UHPCFST structures, having undergone high-temperature damage, experience a significant reduction in bearing capacity, inevitably losing some of their original structural functionalities. Continuing to use such damaged structures poses a severe threat to human safety. However, demolishing post-fire buildings can lead to unnecessary resource wastage and environmental pollution. Therefore, assessing the residual load-bearing mechanical performance of structures after a fire is crucial for their sustainable development. Current research on UHPCFST components mainly focuses on static performance, with only a few investigations on their residual post-fire performance. To the authors' best knowledge, the research on their residual performance after fire incidents during the construction phase has not yet been reported, limiting the application of such structures in high-rise and super high-rise buildings.

In light of this, this study conducts axial compression tests on short UHPCFST columns exposed temperatures during the construction phase, analyzing the residual mechanical performance such as historical maximum temperatures over time, load-deformation curves, strength, and stiffness of UHPCFST components with different aggregate contents and ages after experiencing two types of fires. Furthermore, a formula for calculating the residual bearing capacity of UHPCFST stub columns after high temperatures during the construction phase is proposed.

## 2 Test program

### 2.1 Specimen design

To meet the needs of different fire scenarios, standard guidelines offer standard fire curves for specific situations. Table 1 and Figure 2 summarize the typical standard fire curve alongside pertinent fire scenarios. Specifically, the outdoor standard fire is suitable for scenarios where building components are exposed to either outdoor fires or indoor fires that exhibit significant heat diffusion, indicative of a milder level of fire exposure. For construction sites, scenarios often include a range of combustible materials, good ventilation, and significant heat diffusion, meeting the criteria for a outdoor heating regime. Thus, the outdoor standard fire is applicable for studying fires during the construction phase.

Table 1 Typical standard fire

| Fire system | Formula | Conditions |
|---|---|---|
| ISO 834[28] | $T = 345log_{10}(8t+1)+T_0$ | General indoor environment background, fiber-type fires |
| ASTM E119[29] | $T = 20+750(1-e^{-3.79553\sqrt{t/60}})+170.41\sqrt{t/60}$ | Standard temperature rise curve for American building materials fire resistance tests, applicable to brick and structural material composites in construction |
| Outdoor Fire[30] | $T = 660(1-0.687e^{-0.32t}-0.313e^{-3.8t})+T_0$ | Scenarios where building components are scorched by outdoor fires or where there is substantial heat diffusion in indoor fires, lower level of fire exposure |
| Electrical Fire[30] | $T = 1030\left(1-0.325e^{-0.167t}-0.675e^{-2.5t}\right)+T_0$ | Locations such as power stations and electricity transmission facilities, with organic polymers as the main fuel |
| Hydrocarbon Rise[30] | $T = 1080\left(1-0.325e^{-0.167t}-0.675e^{-2.5t}\right)+T_0$ | Buildings in the petrochemical industry or offshore oil industry, with liquid hydrocarbons as the main fuel |
| Tunnel fire[30] | $T=\begin{cases}\frac{1200-T_0}{5t}+T_0 & 0<t\le 5\\ 1200+T_0 & 5<t\le N\\ 1200-\frac{1200-T_0}{110(t-N)}+T_0 & N<t\le N+110\end{cases}$ | Fully enclosed tunnels along urban subway, highway, and railway routes |

Where, T is the temperature at any given time t (°C); $T_0$ is the initial ambient temperature (°C); T is the duration of the fire (min); N is the sum of the heating and constant temperature phases (min).

Considering the varying degrees of fire exposure depending on the distance from the fire source, Wei[31] conducted numerical simulations of fires in multi-story buildings under construction with different scenarios. It was found that temperatures near and far from the fire source stabilized at around 700℃ and

300°C, respectively. Zhou[32] and Yang[33] also conducted numerical simulations and smoke flow analyses of fires in buildings under construction, noting that temperatures in smaller fires, farther from the fire source, are around 300°C. Based on the outdoor fire temperature rise curve from the GB/T26784-2011[30], two heating regimes, i.e., T1 and T2 are considered. T1 represents scenarios far from the fire source, which is obtain by modifying the the outdoor fire temperature rise curve, as depicted and detailed in Figure 3a. T2 directly utilizes the outdoor fire temperature rise curve to simulate scenarios closer to the fire source, with its graphical representation shown in Figure 3b. For comparative purposes, a control group maintained at normal temperatures (T0) with varying ages is used for benchmarking.

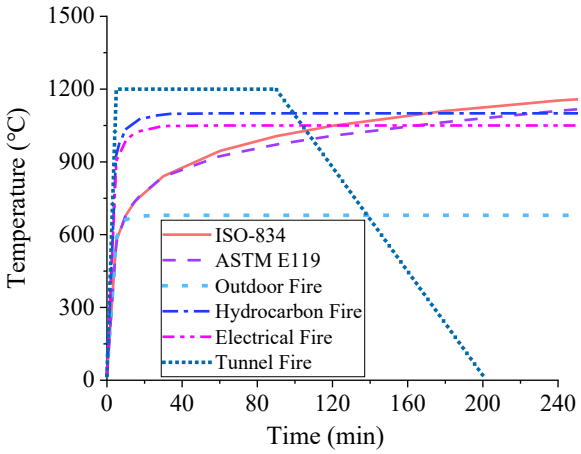


Figure 2 Typical standard fire curve

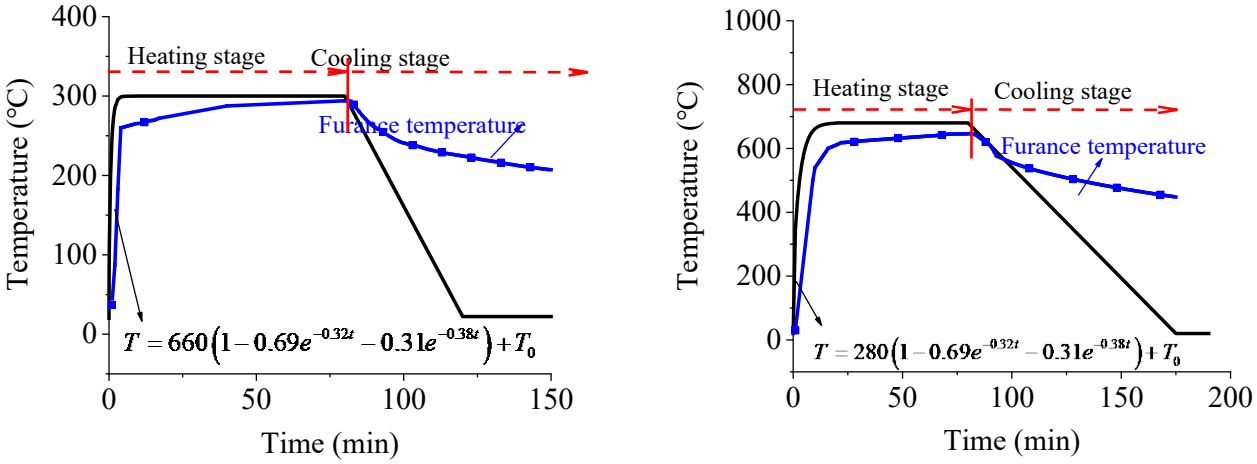


a) T1 b) T2

Figure 3 Heating mode

In accordance with the methodologies reported in the previous research undertaken by the authors[13], the current investigation employs steel tubes with a nominal diameter of 108 mm and a total height of 324 mm. Detailed specifications concerning the dimensions of these steel tubes can be found in Table 2. The

focal point of this study is the core material composed of UHPC, with particular attention to the role of coarse aggregates of various volume ratios, i.e., 0%, 15%, and 30%. The temporal scope of the experiment spans ages of 3, 7, 14, and 28 days. Each specimen is designated using the nomenclature CAi-Tj-Dk, wherein 'CA' signifies Coarse Aggregate, 'i' identifies the specific volume fraction, 'T' represents the temperature treatment protocol, 'j' the particular protocol, and 'D' denotes the age exposed to elevated temperature, with 'k' specifying the exact day count. Table 2 presents further elaboration on the design specifics.

Table 2 The details of the specimens

| Specimen ID | Steel tube | | | | Core UHPC | | Heating mode |
|---|---|---|---|---|---|---|---|
| | Dimensions | | | Properties | Volume fraction | Properties | |
| | $D$(mm) | $H$(mm) | $ds$(mm) | $f_s$ (MPa) | $V_{ca}$ | Stregnth (MPa) | |
| CA00-T0-XXd | 108 | 324 | 4 | 392 | 0% | 115 | T0 |
| CA15-T0-XXd | 108 | 324 | 4 | 392 | 15% | 131 | T0 |
| CA30-T0-XXd | 108 | 324 | 4 | 392 | 30% | 140 | T0 |
| CA00-T1-XXd | 108 | 324 | 4 | 392 | 0% | 115 | T1 |
| CA15-T1-XXd | 108 | 324 | 4 | 392 | 15% | 131 | T1 |
| CA30-T1-XXd | 108 | 324 | 4 | 392 | 30% | 140 | T1 |
| CA00-T2-XXd | 108 | 324 | 4 | 392 | 0% | 115 | T2 |
| CA15-T2-XXd | 108 | 324 | 4 | 392 | 15% | 131 | T2 |
| CA30-T2-XXd | 108 | 324 | 4 | 392 | 30% | 140 | T2 |

Note: $H$, $D$, and $ds$ represent the height, diameter, and thickness of steel tube; $V_{ca}$ refers to coarse aggregate volume fraction.

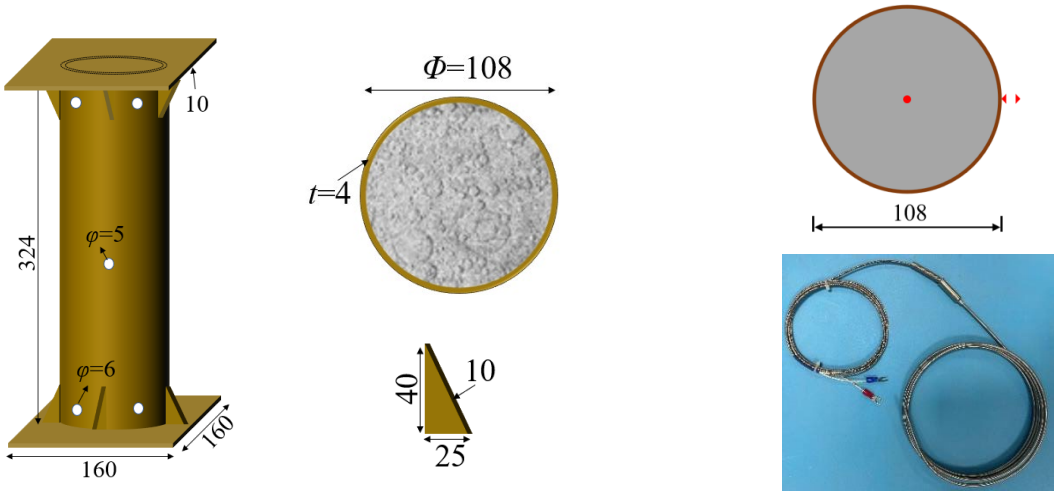


a) Geometry b) Temperature measurement

Figure 4 Geometry of UHPCFST column and temperature measurement

## 2.2 Materials

The raw materials used in the preparation of UHPC include: cement (C), coarse aggregate (CA), sand (S), silica fume (SF), fly ash (FA), steel fibers (SF), polypropylene fibers (PPF), water (W), and high-range water

reducers (WR). Table 3 provides further details of the raw materials.To account for the impact of coarse aggregate, three levels of coarse aggregate volume contents, i.e., 0%, 15%, and 30%, are chosen. In reference to the previous mix designs[18-20],[34], a steel fiber volume of 2% was selected to enhance tensile strength, toughness, and crack resistance, particularly under high temperatures. The 0.2% polypropylene fiber was added to mitigate early-age thermal cracking by forming micro-voids that accommodate thermal expansion. Subsequently, according to ASTM standards[35], the slump flow and density of different mix designs was measured. The specific mixture proportion designs and the properties are presented in Table 4.

Table 3 The raw material of UHPC

| Material | Description |
|---|---|
| Cement | 52.5R ordinary portland cement |
| High-efficiency water reducer | Powdery polycarboxylate superplasticizer |
| Sand | 40-70 mesh refined quartz sand |
| Coarse aggregate | 5-10 mm basalt |
| Silica fume | Silicon dioxide content reaches 95% |
| Fly ash | Class I fly ash |
| Polypropylene fiber | Bundled monofilament, 6mm length, tensile strength >486 MPa |
| Steel fiber | Length 12-14mm, diameter 0.2mm, tensile strength >2000 MPa |
| Water | Tap water |

Table 4 Mixture proportions of UHPC and the properties (kg/m$^3$)

| | Mixture proportions | | | | | | | | | Properties | |
|---|---|---|---|---|---|---|---|---|---|---|---|
| | Cement | Silica fume | Fly ash | Water | Water reducer | Steel fiber | PP fiber | Sand | Coarse aggregate | Slump flow (mm) | Density (kg/m$^3$) |
| CA00 | 857.1 | 107.1 | 107.1 | 182.1 | 11.8 | 157 | 1.9 | 1178.5 | 0 | 621 | 2532 |
| CA15 | 725.7 | 90.7 | 90.7 | 154.2 | 10 | 157 | 1.9 | 997.8 | 375 | 563 | 2624 |
| CA30 | 594.2 | 74.3 | 74.3 | 126.3 | 8.2 | 157 | 1.9 | 817 | 750 | 522 | 2712 |

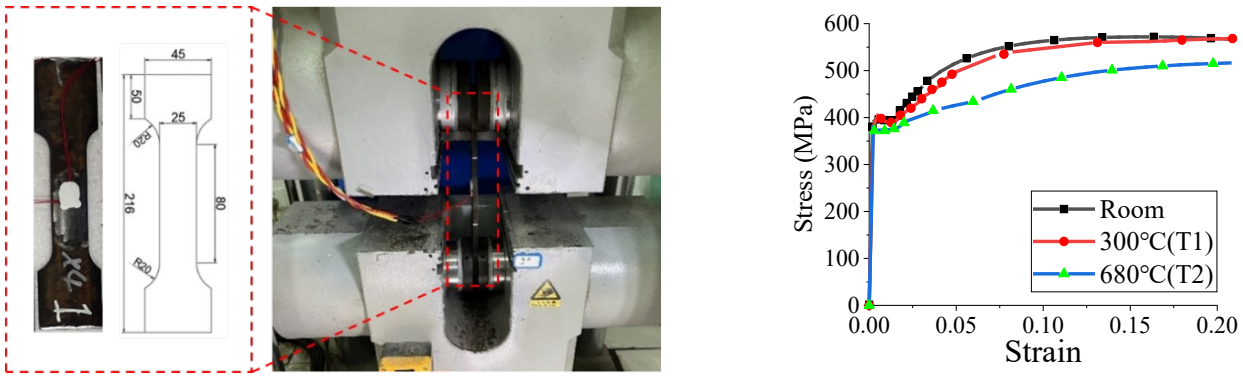


a) Material property testing of steel b) Stress-strain curve

Figure 5 Mechanical performance of steel pipes

A section of steel pipe from the same batch was sampled to prepare the specimen for material property

tests. The dimensions and actual image of the sample are shown in Figure 5 a. In accordance with the standard steel pipe testing methods[36] , the tensile mechanical properties of the steel pipes were tested at room temperature and after exposure to temperatures of 300°C and 680°C. The corresponding stress-strain curves are presented in Figure 5 b. At room temperature, the yield strength of the steel material is 392.4 MPa, and after exposure to 300°C and 680°C, the yield strengths are 391.8 MPa and 372.4 MPa, respectively.

### 2.3 Test process

The experimental procedures comprised both a heating and a loading test, conducted at the Structural Engineering Laboratory at Wuhan University. The custom-built electric furnace utilized in the experiments, depicted in Figure 6 a, can reach temperatures up to 1200°C with an accuracy of ±0.5°C, allowing for precise control during specimen heating.

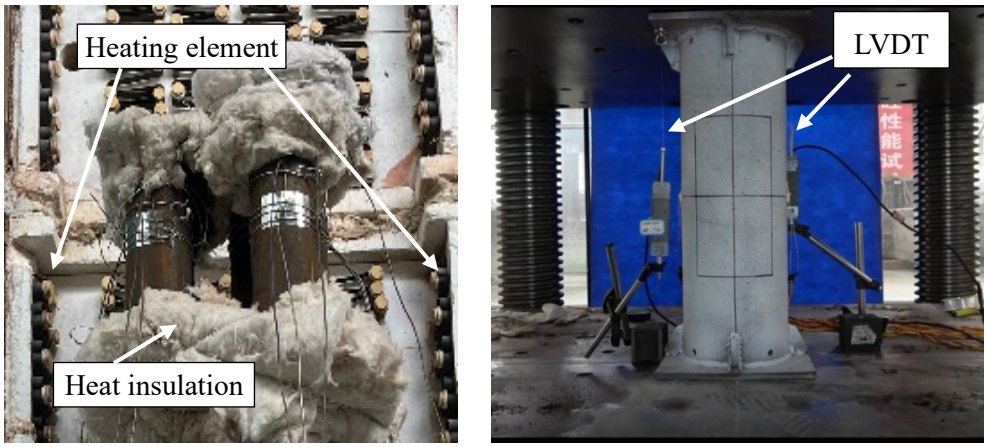


a) Heating test b) Axial compression test

Figure 6 Test process

Prior to the heating tests, the specimens were weighed, then subjected to the predetermined heating regimes. To minimize thermal transfer through the support plates, the top and bottom ends of the specimens were insulated with refractory cotton. Throughout the heating process, the temperatures of both the specimen and the furnace interior were recorded. Subsequent to the heating test, the specimens were weighed again. Figure 3 shows a comparison of the target heating trajectory against the actual temperature inside the furnace, demonstrating a high degree of correlation during the initial heating and early cooling phases. Notably, in the latter stages of cooling, the furnace temperature decreased with a much slower rate than anticipated, attributable to the efficient thermal retention of the furnace. Nevertheless, this discrepancy was observed to have negligible impact on the maximum historical temperatures experienced by the

specimen cross-sections.

Figure 6 b illustrates the testing setup where an electro-hydraulic servo-controlled compression up to 30000 kN was employed to apply an axial load on the test specimens. The axial deformation was quantified using an array of two linear variable differential transformers (LVDTs), strategically positioned to ensure precise measurement. In the preliminary stages, each specimen underwent a preload phase to confirm the centrality of the load application. This critical step was validated by analyzing and comparing the readings from all two LVDTs for consistency. Once centered loading was assured, the specimens were incrementally loaded at a steady rate of 1 mm/min. The process continued until the specimens reached a compressive strain threshold of between 40000 and 50000 microstrain (με), ensuring that the load was applied uniformly and the deformation was measured accurately throughout the testing regime.

# 3 Test results and discussion

## 3.1 Temperature responses

### 3.1.1 Thermal mass loss

Figure 7 and Figure 8 present the mass loss and mass loss rate (the ratio between mass loss and initial mass) of the specimens exposed to elevated temperatures at different ages. It is evident that under the T1 heating regime, the mass loss rate increases with the progression of the fire exposure period. This can be attributed to the fact that at earlier ages, relatively lower temperatures (approximately 200 ℃) are more likely to promote hydration reactions, thus resulting in less water loss. When subjected to T2,the historical-max of core UHPC is round 500 ℃ the mass loss rate is significantly greater than under the T1 regime. Additionally, it is observed that the mass loss rate tends to decrease as the age increases, which may be due to the earlier aged specimens more readily undergoing dehydration under higher temperature conditions. Furthermore, it is noted that due to the high thermal stability of basalt, the mass loss rate decreases as the content of coarse aggregate increases.

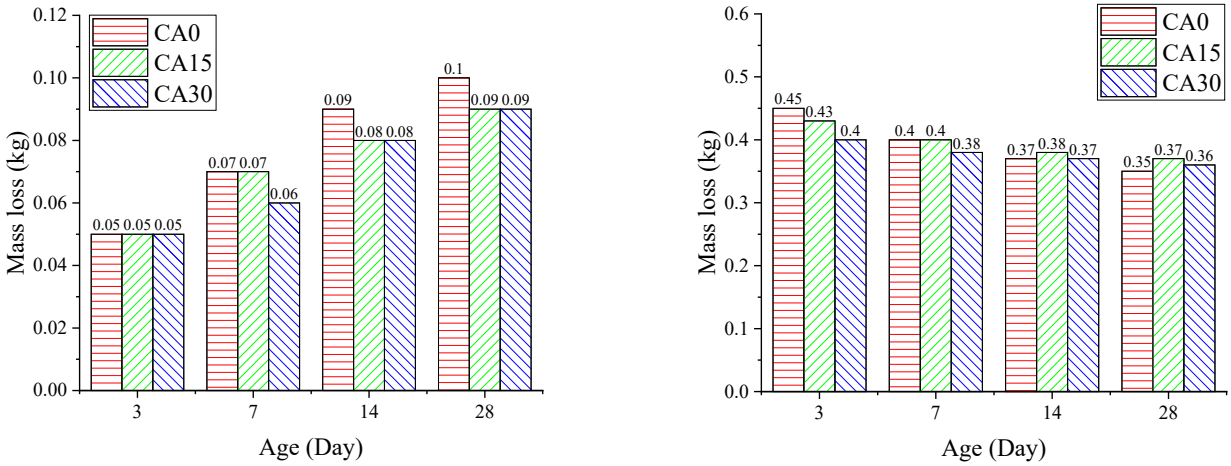


a) T1 b) T2

Figure 7 Mass loss

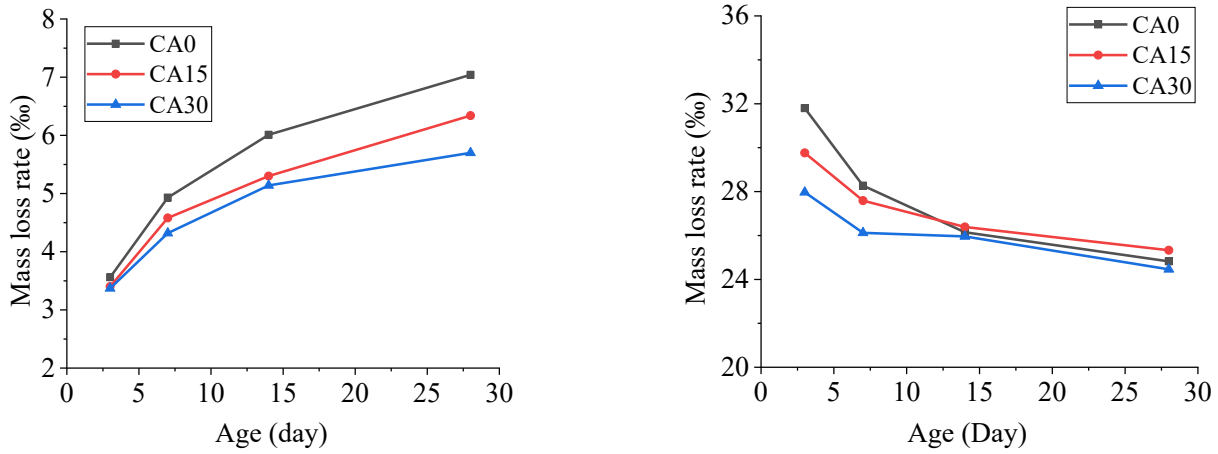


a) T1 b) T2

Figure 8 Mass loss rate

### 3.1.2 Real-time temperature curve and historical-max temperature

Figure 9 shows the real-time temperature curve of the furnace, outer steel tube and core UHPC of the specimen, it can be found that the temperature curves across the specimens with different parameters do not display significant variations. To better understand the influence of the parameters on the temperature response, the historical-max temperature of both the steel tube and the core UHPC were derived from the real-time temperature, which are presented in Figure 10. It can be found that the historical-max temperatures of both the steel tube and the core UHPC increase with age of UHPC exposed to elevated temperature. This trend is particularly pronounced for the core UHPC, primarily due to the reduction in the amount of free water inside the UHPC as it ages, resulting in less heat absorbed by water dissipation at the same temperature. Additionally, it's observed that with an increased proportion of coarse aggregate, the

historical-max temperature of both the steel tube and the UHPC gradually rise across different ages. This phenomenon is attributed to the higher thermal conductivity of coarse aggregates compared to mortar, facilitating easier heat transfer to the UHPC interior. Furthermore, the lower specific heat capacity of coarse aggregates means that they have absorbed less heat during the temperature rise, thereby resulting in higher surface temperatures of the steel tube in the corresponding specimens.

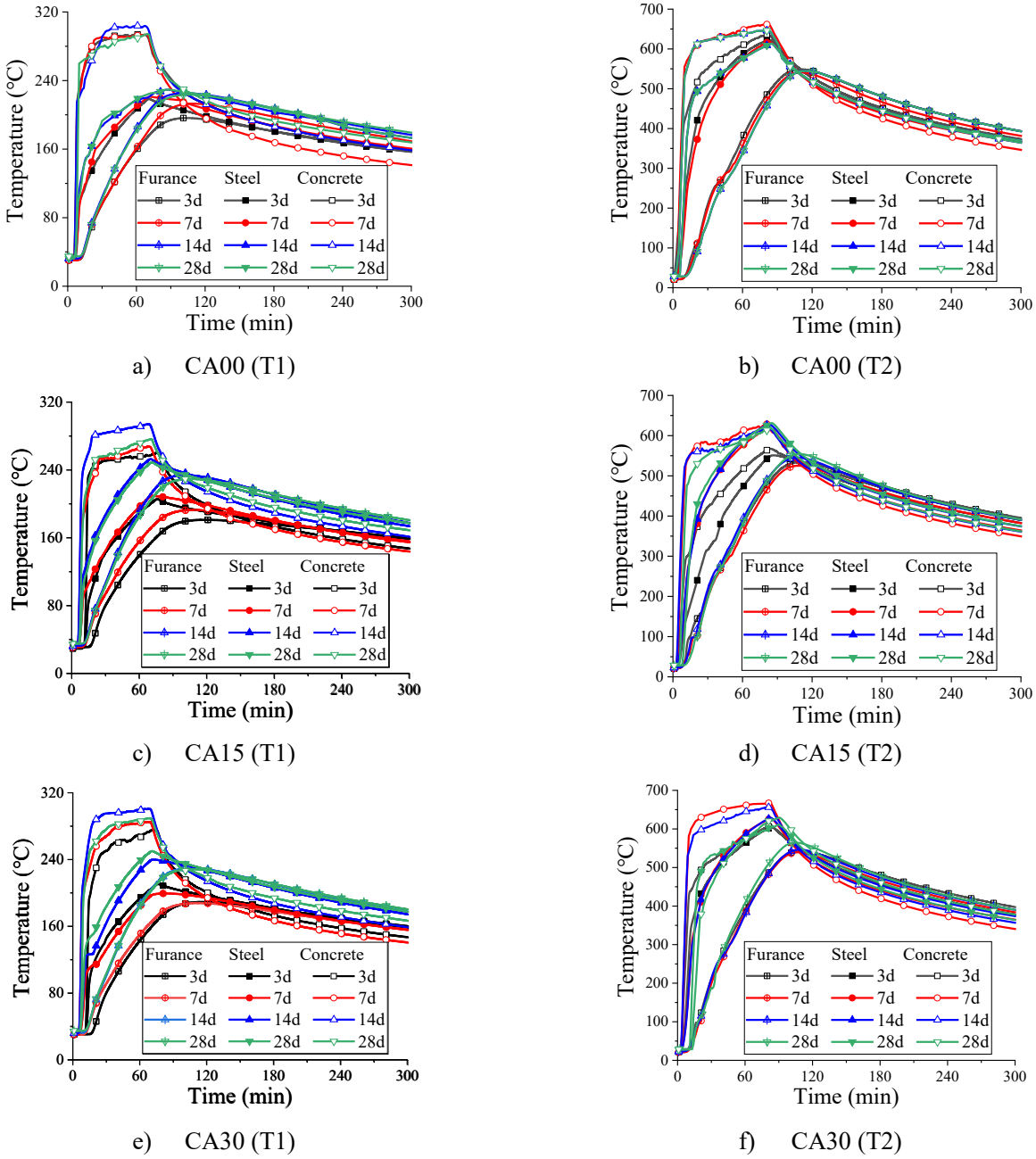


a) CA00 (T1) b) CA00 (T2)

c) CA15 (T1) d) CA15 (T2)

e) CA30 (T1) f) CA30 (T2)

Figure 9 Real-time temperature curve

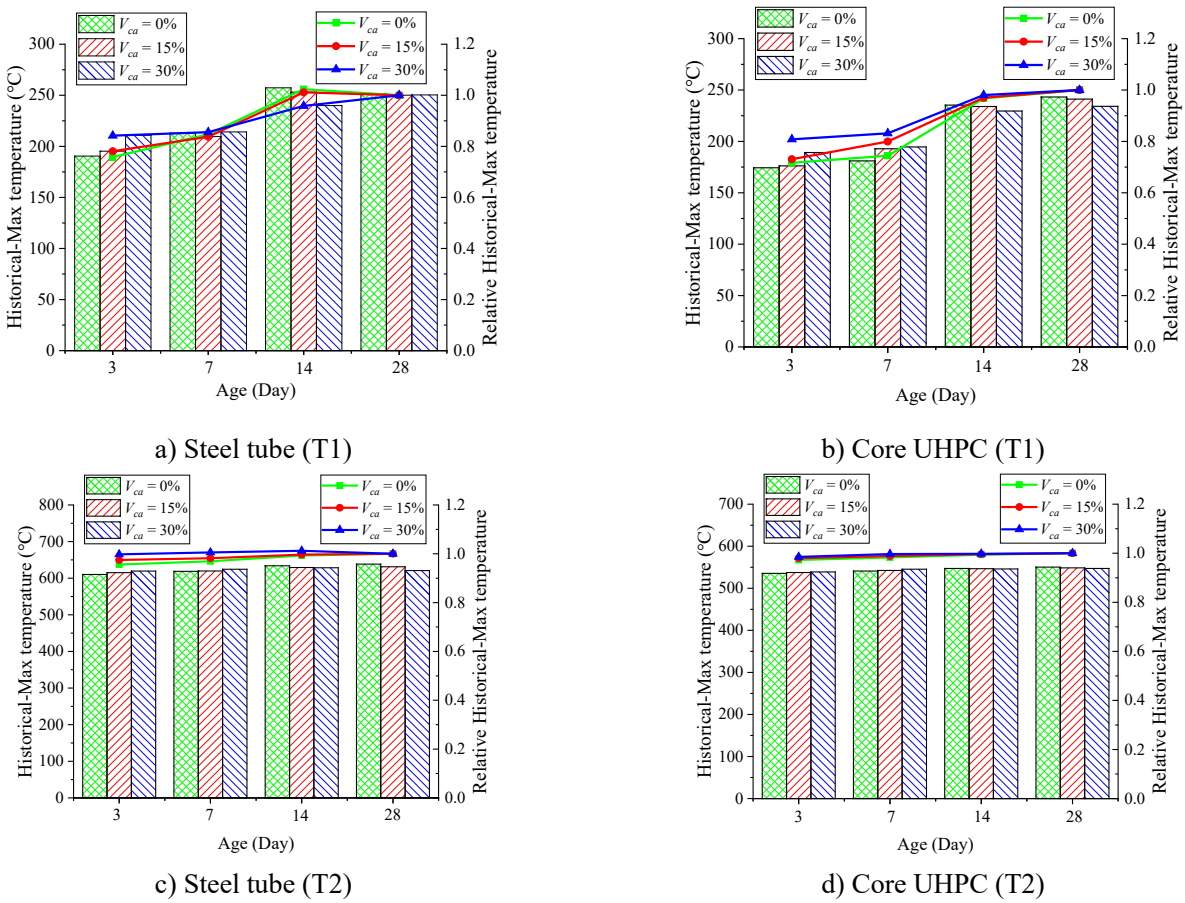


a) Steel tube (T1)

b) Core UHPC (T1)

c) Steel tube (T2)

d) Core UHPC (T2)

Figure 10 Historical-max temperatures of steel tube and core UHPC

## 3.2 Mechanical response

### 3.2.1 Failure modes

Figure 11 presents the failure modes of the UHPCFST columns exposed to elevated temperatures at different early age, revealing two distinct patterns: shear and drum-shaped bulging. The shear mode was characterized by local bulging at both ends of the steel tube and a pronounced diagonal fracture within the concrete core upon tube removal. The drum-shaped bulging mode was characterized by several minor protrusions distributed along the length of the steel tube, while the UHPC core remained predominantly intact without visible cracking. It was observed that the UHPCFST specimens with lower maturity, specifically those at 3 and 7 days, predominantly failed in a drum-shaped bulging manner due to the robust confinement by the external steel tubes. As the UHPC matured and the strength increased, the failure mode of the specimens was transitioned to shear failure, a consequence of the relatively reduced confinement effect of the steel tubes. Following the T1 thermal exposure, diagonal shear failure was uniformly observed across the specimens. This was attributed to the enhancement of UHPC strength before 300℃, while the

strength of steel remained largely static, thus providing inadequate confinement. The overall failure mode was governed by the core UHPC, where axial compression created a non-uniform, triaxial stress state. Localized shear stress concentrations exceeded the UHPC's shear capacity, leading to diagonal cracks and resulting in shear-dominated failure of the UHPCFST specimens.

In contrast, under the T2 thermal exposure, the core UHPC is exposed to temperatures between 500 ℃ and 600 ℃, higher than T1, leading to a significant reduction in its strength compared to T1. However, after exposure to both T1 and T2 high-temperature conditions, the steel recovers to a strength close to that observed at room temperature. Consequently, under T2 conditions, the steel tube provides a relatively higher confinement effect to the weakened UHPC core, resulting in bulging failures.

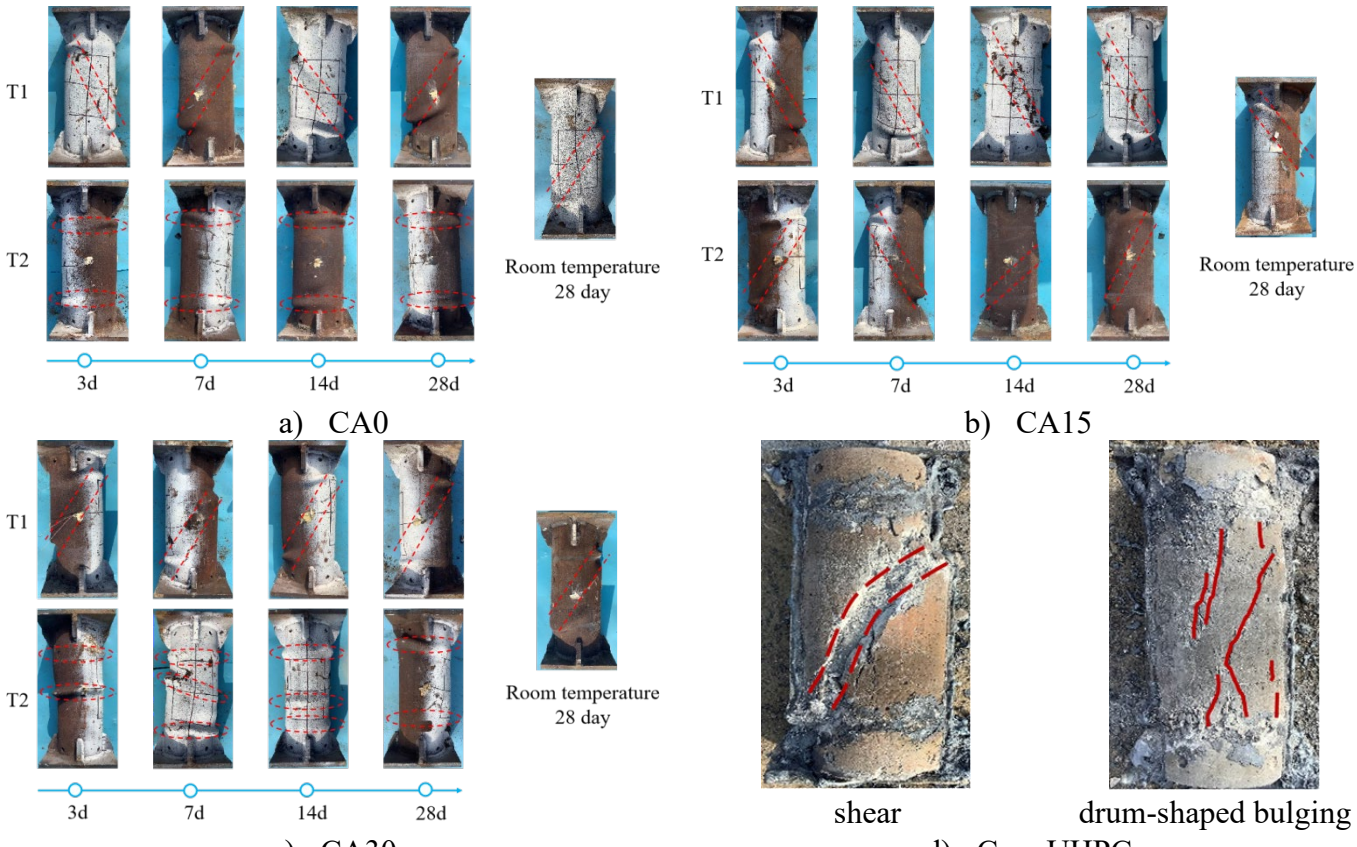


Figure 11 Failure modes of the specimens

After removing the steel tube from the concrete, the failure pattern of the core UHPC is as shown in the Figure 11d. Despite the presence of large cracks on the surface of the core UHPC, these cracks predominantly result from the progression of externally applied loads. Notably, no explosive spalling is observed, even though UHPC is highly susceptible to spalling under high temperatures[37, 38]. This absence of spalling can be attributed to the confining effect of the external steel tube, which mitigates the stress induced by steam pressure and thermal expansion, thereby preventing the initiation of explosive failure.

### 3.2.2 Load-deformation curves

The load-deformation curves for all the specimens are shown in Figure 12. Based on the curve characteristics, the curves can be classified into three types as illustrated in Figure 13.

In the specimens with greater maturity at ambient temperature, the core UHPC demonstrates elevated strength, with comparatively limited constraint from the steel tube. The corresponding load-deformation curve can be categorized into four distinct phases:1) Initial Elastic Stage (OA): The steel tube and the UHPC core are elastic. The steel tube shows greater circumferential deformation due to a higher Poisson's ratio than the UHPC core, leading to minimal constraint on the UHPC. 2) Elastic-Plastic Stage (AB): As the load nears the ultimate limit, both components enter the plastic phase. The steel tube yields, transferring most of the load to the UHPC core, which remains elastic but develops micro-cracks. 3) Descending Stage (BC): Upon reaching its strength limit, the behavior of the UHPC core changes. With minimum constrains, the core is sheared into wedges with sharp load reduction. When constrained by the steel tube, crack development is slower, and load drop is less abrupt. 4) Gentle Ascending Stage (CD): As the lateral deformation of the UHPC core increases, the constraining effect of the steel tube also increases, maintaining the load capacity of the core. The steel tube strengthens with increased deformation, enhancing the overall load capacity of the UHPC within. This curve is classified as Type-I.

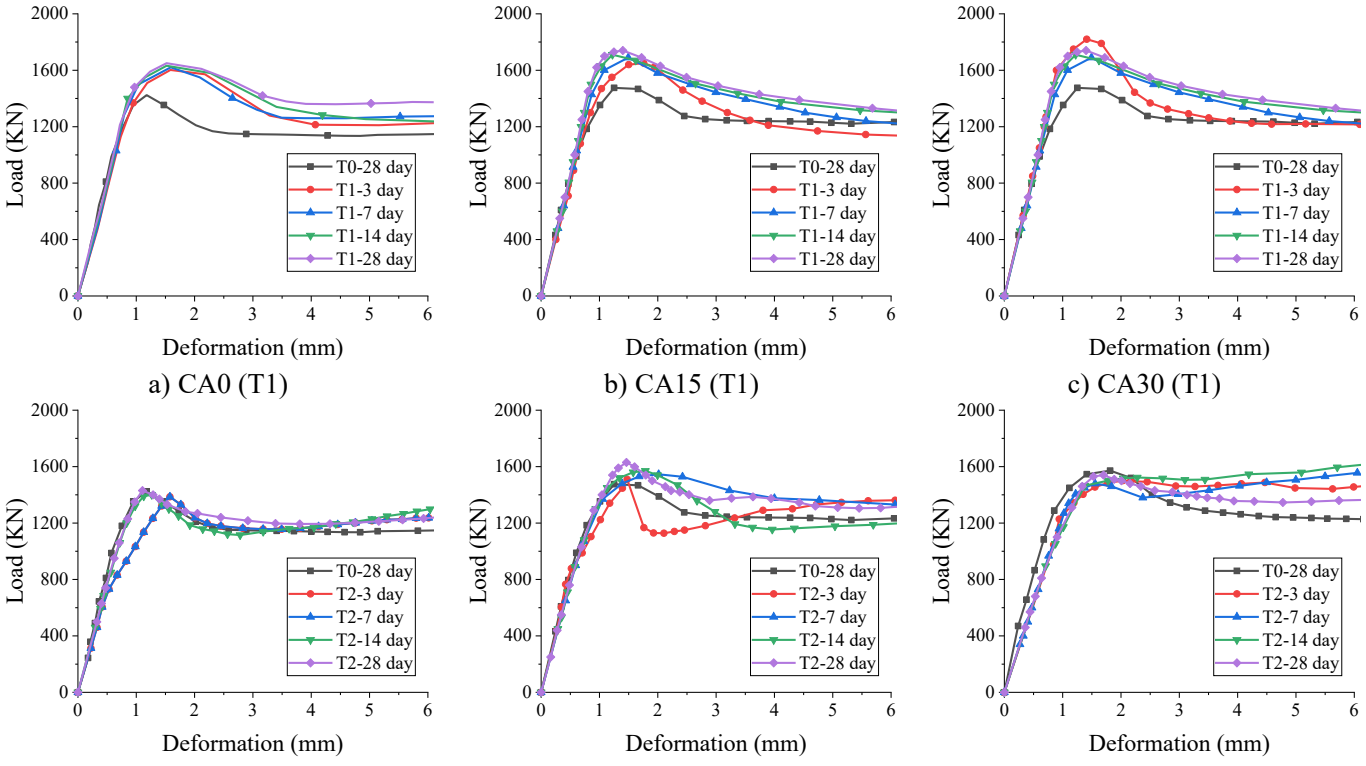


a) CA0 (T1) b) CA15 (T1) c) CA30 (T1)

d) CA0 (T2) e) CA15 (T2) f) CA30 (T2)

Figure 12 Load-deformation curve of UHPCFST columns

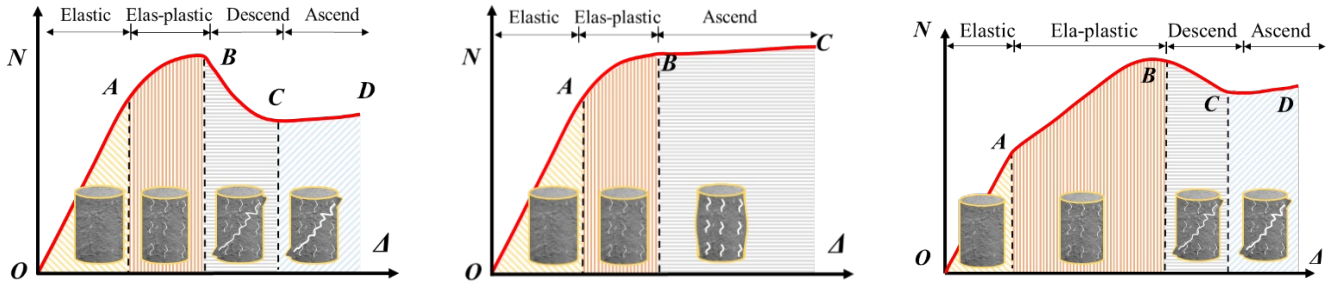


a) Type-I b) Type-II c) Type-III

Figure 13 Typical load-deformation curve of UHPCFST columns

For specimens with lower maturity at ambient temperature, the core strength of the UHPC is reduced, thereby enhancing the confining effect of the external steel tube. When the concrete fails, the steel tube offers greater restraint, suppressing the propagation of internal cracks in the concrete. These specimens display a bulging failure mode that is classified as Type-II. Unlike Type-I, these specimens feature a load-deformation curve that progresses directly upward without a descending phase after the elastic-plastic stage, due to the substantial constraining effect of the external steel tube. Therefore, the difference between Type-I and Type-II specimens lies in the concrete core strength and the confinement provided by the steel tube, leading to the different post-peak behavior.

Specimens subjected to T2 thermal curves, with a relatively higher residual strength of the core UHPC, also display shear failure. Compared to Type-I and Type-II specimens, the elastic modulus of the core UHPC in Type-III specimens significantly deteriorates, for the core UHPC is exposed to temperatures between 500 and 600 °C. However, the external steel tube experiences minimal change in stiffness after cooling from high temperatures. As a result, the relative stiffness of the steel tube increases in comparison to the softened UHPC core. Consequently, during the elastic phase, the steel tube carries a greater portion of the axial load, yielding prematurely. Compared to a Type-I specimen, the load-deformation curve of this category, due to the early yielding of the steel tube, exhibits a shorter elastic stage and a prolonged elastic-plastic phase, and is classified as Type-III.

### 3.2.3 Residual bearing capacity

The residual bearing capacity after fire is one of the important indicators of the post fire mechanical performance of UHPCFST column. For components with a distinct descending phase in the load-deformation curve, the peak load is taken as the residual bearing capacity of the component. For components without a distinct descending segment, the residual bearing capacity is determined using the farthest point method as reported in reference[39].

Figure 14 presents the bearing capacity of all the UHPCFST columns. To facilitate the analysis of the residual performance of UHPCFST columns after elevated temperature during construction, this paper also defines the relative bearing capacity coefficient of UHPCFST columns as $k_N$.

$$k_N = \frac{N_{T_{max}}}{N_{0,28}} \tag{1}$$

where $N_{0,28}$ is the 28-day bearing capacity of the UHPCFST column at room temperature.

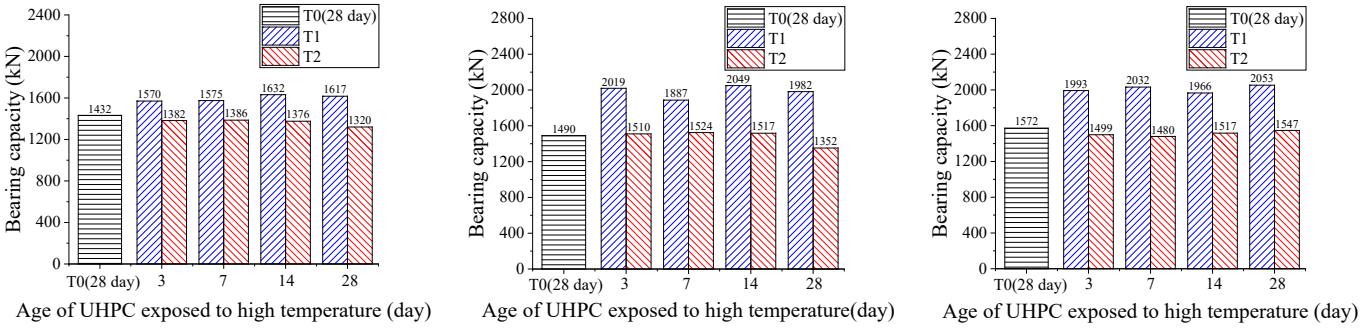


a) CA0 b) CA15 c) CA30

Figure 14 Bearing capacity of the UHPCFST column

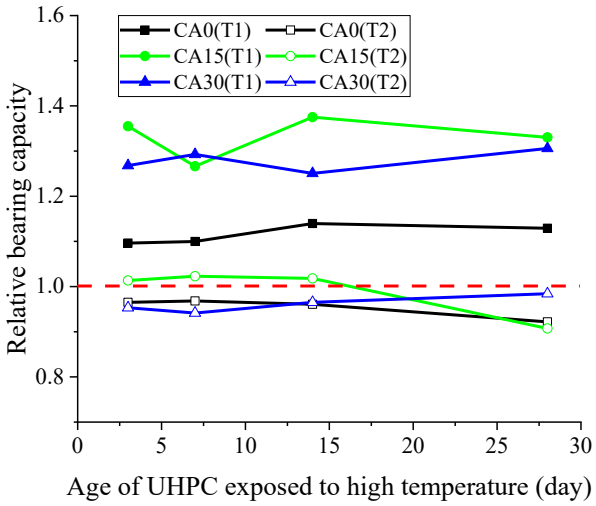


Figure 15 Relative bearing capacity of the UHPCFST column

Figure 15 shows the relative bearing capacity of the UHPCFST column. It can be found that the relative bearing capacity of all the specimens exposed to elevated temperature at different early-age under the T1 heating regime is greater than 1.This improvement is largely attributed to the core UHPC subjected to peak temperatures between 150~300°C. The high-temperature curing effect significantly promotes hydration and pozzolanic reactions[40], resulting in a net gain in strength, while the predominant losses are

free water and gel water[41], accompanied by minimal decomposition of hydration products. Therefore, both the core UHPC and the UHPCFST columns demonstrate an increase in overall strength. At the same time, it can be observed that the overall bearing capacity of the column shows an increasing trend with the growth of the high-temperature aging period. It is attributable to the fact that early-aged UHPC has weaker resistance to high-temperature deterioration, leading to more severe damage after exposure, although high temperatures accelerate hydration and pozzolanic reactions. Under the T2 heating regime, most of the relative strength of the test specimens is smaller than 1 for that the core UHPC has experienced peak temperatures exceeding 500°C, where the detrimental effect of high-temperature damage outweighs the hydrating promotion effect, leading to a reduction in the strength of the core UHPC. Additionally, it is observed that the overall bearing capacity of the column exhibits a decreasing trend with the growth of the high-temperature aging period.

### 3.2.4 Residual Stiffness

The compressive stiffness of the investigated composite section was designated as the secant stiffness corresponding to a column strength of 0.4 time[42] . Figure 16 presents the stiffness of all the tested UHPCFST columns. As expressed in Eq.(2), This study defines the relative stiffness of UHPCFST columns as the ratio between the stiffness of a structural component and that of the corresponding fully matured component under ambient temperature conditions (Room temperature, 28 days).

$$k_E = \frac{E_{T_{max}}}{E_{0,28}} \tag{2}$$

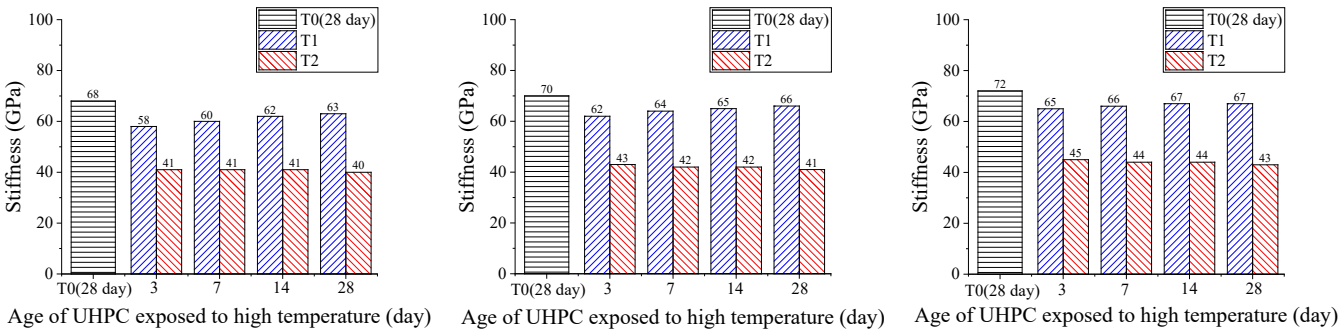


a) CA0 b) CA15 c) CA30

Figure 16 Stiffness of the UHPCFST column

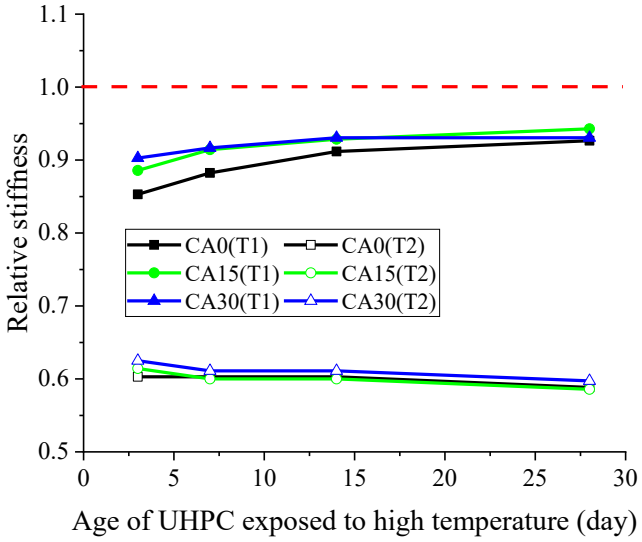


Figure 17 Relative stiffness of UHPCFST columns

The relative stiffness of the UHPCFST columns is illustrated in Figure 17. It is evident that under the T1 heating regime, in comparison to the components matured at ambient temperature, their stiffness is slightly reduced, with a relative stiffness ranging between 0.85 and 0.95. Furthermore, the overall stiffness of the columns exhibits an increasing trend with the duration of high-temperature aging. Similarly, under the T2 heating regime, compared to the components matured at ambient temperature, their stiffness experiences a more noticeable reduction, with a relative stiffness ranging between 0.55 and 0.65. Moreover, the overall stiffness of the columns demonstrates a decreasing trend with the duration of high-temperature aging.

## 4 The calculation of the residual bearing capacity

### 4.1 The exciting model of calculating the residual bearing capacity of CFST

Calculating the residual bearing capacity of concrete-filled steel tubes (CFST) after exposure to high temperatures is critically important for ensuring the structural integrity and safety of buildings post-fire. This process is characterized by its complexity, as it involves accounting for the uneven heat damage to the materials. As listed in Table 5, the previous researchers, including Yang[43], Jiang[44], Li[45], and Lv[46] have proposed empirical methods for calculating the residual bearing capacity of CFST after exposed to elevated temperature based on the experimental and simulation results. These formulas are susceptible to the quality of regression samples and the range of parameters. Additionally, these models are generally based on standard temperature rise curves, necessitating re-fitting when temperature regimes vary.

Table 5 Practical calculation formula for the residual bearing capacity of CFST columns after fire

| Formula source | Specific formula |
|---|---|
| Yang[43] (2005) | $k_r=\begin{cases}(1-0.09t_0)\cdot f(D_o)\cdot f(\lambda_0)\cdot f(n_0) & t_o\le 0.3\\(-0.56t_0+1.14)\cdot f(D_0)\cdot f(\lambda_0)\cdot f(n_0) & t_o>0.3\end{cases}$ |
| Jiang[44] (2009) | $k_r=\begin{cases}(1.0035-0.09t_0)\cdot f(D_o)\cdot f(\lambda_0) & T\le 300℃\\(1.2634-0.0008t_0)\cdot f(D_0)\cdot f(\lambda_0) & T>300℃\end{cases}$ |
| Li[45] (2015) | $k_r=1-\left(6.41f_r^4-12.68f_r^3+6.88f_r^2+0.12f_r\right)$<br>$f_r=f(t_o)\cdot f(a_o)\cdot f(D_o)$ |
| Lv[46] (2018) | $k_r=\left(7.215f_s+6.056f_{ck}+12300\alpha-100t_0+3.353D_0\right)\times10^{-5}+0.936$ |

Note: $k_r$ represents the reduction factor of the residual bearing capacity of CFST components after high temperature, which is the ratio of residual bearing capacity after high temperature to the bearing capacity at normal temperature.

$t_0$、$D_o$、$\lambda_0$、$n_0$、$a_0$、$\alpha$、$f_s$、$f_{\mathrm{ck}}$ respectively represent the heating time, cross-sectional diameter, slenderness ratio, load ratio, protective layer thickness, steel content, yield strength of steel, and axial compressive strength of core concrete.

In our previous work[20], a method for calculating the residual bearing capacity of CFST columns at mature age was proposed based on the average historical-max temperature (AHT),where the unevenly heat-damaged material is effectively considered as a uniformly damaged material by employing the AHT approach and the residual bearing capacity of CFST columns can be expressed as Eq.(3).

$$N_{T_{max}}=\iint_{A_\alpha} f_{\alpha,T_{max}}\left(T_{\alpha,T_{max}}\right)dA=\overline{f}_{\alpha,T_{max}}\left(\overline{T}_{\alpha,T_{max}}\right)A_\alpha \tag{3}$$

where $N_{T_{max}}$ is the residual bearing capacity, $T_{\alpha,T_{max}}$ and $\overline{T}_{\alpha,max}$ are the historical-max temperature and average historical-max temperature, respectively. $f_{\alpha,T_{max}}$ and $\overline{f}_{\alpha,T_{max}}$ are the material's original reduction factor and equivalent reduction factor, the subscripts $\alpha$ taking c and s refer to concrete and steel, respectively.

To calculate the residual bearing capacity of the post-fire UHPCFST column based on the AHT method, there are three main steps:

Step1: Calculate average historical-max temperature of steel tube ($\overline{T}_{s,max}$) and core UHPC ($\overline{T}_{c,max}$), respectively.

Step2: Calculate equivalent strength of the steel ( $\overline{f}_{s,T_{max}}$ ) tube and the concrete core ( $\overline{f}_{c,T_{max}}$ ) at the average temperatures from step 1, respectively.

Step3: Calculate post-fire residual strength of the UHPCFST columns ( $N_{T_{max}}$ ) by substituting the residual equivalent strengths of the steel tube and concrete into the bearing capacity formula used for room temperature conditions.

By following these steps, the residual bearing capacity of UHPCFST columns after fire exposure can be evaluated using the AHT method. In this approach, the calculation processes for historical-max temperature and strength degradation due to temperatures are decoupled, thus providing a theoretically robust and compatible method for post-fire assessment.

### 4.2 Establishment of proposed model

Based on the calculation method of the AHT, this paper proposes a formula for calculating the residual bearing capacity of UHPCFST exposed to elevated temperature at early age. The first step of this method involves calculating the AHT of the steel tube and the core UHPC separately. Due to the outer steel tube's thin profile and good heat transfer properties, it exhibits an approximately uniform temperature distribution. Therefore, the AHT of the steel is equivalent to the historical-max temperature at any point on the steel tube. The historical-max temperatures on the surfaces of the steel tubes of each component are listed in Table 6. For the core UHPC, which usually has a thicker cross-section and relatively poorer thermal conductivity, the historical-max temperature field of the core concrete after high temperature exhibits a certain degree of non-uniformity. In this paper, based on the peak temperature of the measured temperature-time curve of the UHPC section, the AHT of the core UHPC for each component is obtained using Eq. (4), as shown in Table 6.

$$\overline{T}_{c,max} = \frac{\int_0^{d_0} T_{max}(d)\mathrm{dS}}{S} \tag{4}$$

where, $T_{max}(d)$ is the historical maximum temperature along the depth; $d_0$ is the distance from the centre to the concrete surface; $S$ is the area of the core UHPC.

The second step of the AHT-based residual bearing capacity calculation method involves determining the equivalent strengths of the steel tube and the core UHPC. Given the steel tube's uniform temperature

due to its good thermal conductivity and thin wall thickness, its post-fire temperature residual equivalent strength is considered to be its original strength. The equivalent strength can be expressed in Eq.(5) referring to the predicted formula for the yield strength of the steel after high temperature by Shi[47].

$$\frac{f_{s,\overline{T}_{max}}}{f_{s,20}}=\begin{cases}1 & \overline{T}_{s,max}\le 500^{\circ}C \\ 0.8441\left(\frac{\overline{T}_{s,max}}{500}-1\right)^4-0.5259\left(\frac{\overline{T}_{s,max}}{500}-1\right)^3-0.4818\left(\frac{\overline{T}_{s,max}}{500}-1\right)^2+1 & 500^{\circ}C<\overline{T}_{s,max}\le 1000^{\circ}C\end{cases} \tag{5}$$

As for the core UHPC, our previous studies have shown that the UHPC's original strength($f_{c,T_{max}}$) and equivalent strength ($\bar{f}_{c,\bar{T}_{max}}$) are quite similar[20]. Therefore, it is assumed that the UHPC's original residual strength is equal to the equivalent residual strength, namely,$f_{c,\bar{T}_{max},t_T}=f_{c,T_{max},t_T}$. Additionally, our research group conducted a experimental study on residual strength of UHPC exposed to high temperature at early age[48], and established a mathematical model considered temperature level ($T_{max}$) and high-temperature aging period ($t_T$),which can be expressed as follows:

$$f_{c,T_{max},t_T}=f_c\times k_{c,T_{max},t_T} \tag{6}$$

$$k_{c,T_{max},t_T}=1+k_{c,T_{max}}\times k_{c,t_T} \tag{7}$$

$$k_{c,T_{max}}=-3.66\left(\frac{T_{max}-20}{1000}\right)^3-7.57\left(\frac{T_{max}-20}{1000}\right)^2+2.76\left(\frac{T_{max}-20}{1000}\right) \tag{8}$$

$$k_{c,t_T}=1-e^{-1.94t_T} \tag{9}$$

where $f_{c,T_{max},t_T}$ is the axial compressive residual strength of early-age UHPC exposed to elevated temperature;$f_c$ is the axial compressive strength of hardened UHPC at room temperature; $k_{c,T_{max},t_T}$is the reduction coefficient for axial compressive strength due to temperature and high-temperature aging; $k_{c,T_{max}}$ is the change of axial compressive strength due to high temperature at mature age. $k_{c,t_T}$ is the development coefficient in UHPC axial compressive strength with the development of the high-temperature aging period.

Additionally, the authors previously provided a formula for calculating the bearing capacity of early-age UHPCFST at room temperature[13].

$$N_0=\left(1+0.3\frac{t}{0.28+0.99t}\frac{\xi_d}{1+\xi_d}\right)\left(A_c f_{c,d}+A_s f_s\right) \tag{10}$$

where, $t$ is UHPC age $\xi_d=(f_sA_s)/(f_{c,d}A_c)$is the confinement factor of outer steel tube, $f_{c,d}$ and $f_y$ are the characteristic compressive strength of early-age concrete and yield strength of steel, respectively. $A_s$ and $A_c$

are the cross-sectional areas of the concrete and steel, respectively.

Finally, replacing the strengths of the steel tube and concrete in the Eq.(10) with the equivalent strengths of the steel tube and concrete after exposure to high temperatures at early age, thus, model for calculating the residual bearing capacity of the UHPCFST columns exposed to elevated temperature can be expressed in Eq.(11) . The predicted results are presented in a Table 6.

$$N_{T_{max}} = \left(1+0.3\frac{t_T}{0.28+0.99t_T}\frac{\xi_{T_{max}}}{1+\xi_{T_{max}}}\right)\left(A_c f_{c,\bar{T}_{\max},t_T} + A_s f_{s,\bar{T}_{\max}}\right) \tag{11}$$

where, $t_T$ is age of UHPC exposed to elevated temperature; $\xi_{\bar{T}_{max}} = (f_{s,\bar{T}_{max}}A_s)/(f_{c,\bar{T}_{max}}A_c)$ is the confinement factor of outer steel tube, $f_{s,\bar{T}_{max}}$ is the equivalent residual yield strength of steel exposed to elevated temperature, $f_{c,\bar{T}_{max},t_T}$ is the equivalent residual compressive strength of early-age UHPC exposed to elevated temperature.

Table 6 The calculation of the bearing capacity of early-age UHPCFST column exposed to elevated temperature

| Specimen ID | AHT of steel tube (℃) $\bar{T}_{s,max}$ | $f_{s,\bar{T}_{max}}$ (MPa) | AHT of UHPC (℃) $\bar{T}_{c,max}$ | $f_{c,\bar{T}_{max},t_T}$ (MPa) | Confinement factor $\xi_{T_{max}}$ | Tests (kN) | Predicted (kN) |
|---|---|---|---|---|---|---|---|
| CA00-T1-3d | 190 | 392 | 182 | 126 | 0.519 | 1570 | 1654 |
| CA15-T1-3d | 195 | 392 | 186 | 164 | 0.397 | 2019 | 1908 |
| CA30-T1-3d | 211 | 392 | 200 | 172 | 0.38 | 1993 | 2014 |
| CA00-T1-7d | 213 | 392 | 197 | 127 | 0.515 | 1575 | 1660 |
| CA15-T1-7d | 210 | 392 | 201 | 165 | 0.394 | 1887 | 1915 |
| CA30-T1-7d | 214 | 392 | 204 | 172 | 0.379 | 2032 | 2016 |
| CA00-T1-14d | 257 | 392 | 246 | 127 | 0.512 | 1632 | 1666 |
| CA15-T1-14d | 253 | 392 | 235 | 166 | 0.392 | 2049 | 1921 |
| CA30-T1-14d | 240 | 392 | 235 | 173 | 0.378 | 1966 | 2022 |
| CA00-T1-28d | 251 | 392 | 247 | 127 | 0.512 | 1617 | 1666 |
| CA15-T1-28d | 250 | 392 | 246 | 166 | 0.392 | 1982 | 1921 |
| CA30-T1-28d | 250 | 392 | 242 | 173 | 0.378 | 2053 | 2022 |
| CA00-T2-3d | 610 | 381 | 535 | 83 | 0.768 | 1382 | 1295 |
| CA15-T2-3d | 615 | 380 | 538 | 107 | 0.592 | 1510 | 1452 |
| CA30-T2-3d | 620 | 379 | 539 | 110 | 0.573 | 1500 | 1508 |
| CA00-T2-7d | 619 | 380 | 541 | 81 | 0.782 | 1386 | 1281 |
| CA15-T2-7d | 620 | 379 | 542 | 105 | 0.599 | 1524 | 1439 |
| CA30-T2-7d | 624 | 378 | 545 | 108 | 0.582 | 1480 | 1491 |
| CA00-T2-14d | 634 | 376 | 547 | 78 | 0.798 | 1376 | 1254 |
| CA15-T2-14d | 629 | 377 | 547 | 103 | 0.608 | 1517 | 1420 |
| CA30-T2-14d | 629 | 377 | 546 | 107 | 0.584 | 1517 | 1485 |
| CA00-T2-28d | 638 | 375 | 550 | 78 | 0.803 | 1320 | 1247 |
| CA15-T2-28d | 631 | 377 | 549 | 103 | 0.611 | 1352 | 1415 |
| CA30-T2-28d | 621 | 379 | 547 | 108 | 0.582 | 1547 | 1495 |

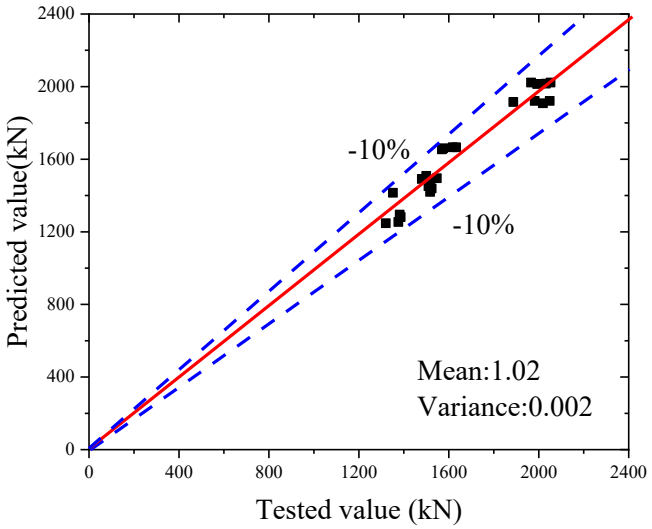


Figure 18 The comparison of bearing capacity between tested and predicted value

Figure 18 presents the comparison of the tested and the predicted bearing capacities of UHPCFST. It can be found that the predicted results match well with the tested, indicating the applicability of the modified AHT method in predicting bearing capacity of the UHPCSFST column after being exposed to elevated temperature at early-age. It should be noted that the proposed equations are specifically designed to predict the residual bearing capacity of UHPCFST exposed to elevated temperature during construction with core UHPC strength at room temperature ranging from 115 to 140 MPa, age from 3 to 28 days.

To further validate the rationality of the proposed method, we utilized our previous tests[20] on the residual bearing capacity of UHPCSFST columns at a matured age. Table 7 provides the detailed calculation process, and Figure 19 illustrates the comparison between the predicted and tested results. The close alignment between the two demonstrates the high reliability and rationality of the proposed method.

Table 7 The calculation of the bearing capacity of UHPCFST column exposed to elevated temperature at matured age

| Specimen ID | AHT of steel tube (℃) $\overline{T}_{s,max}$ | $f_{s,\overline{T}_{max}}$ (MPa) | AHT of UHPC (℃) $\overline{T}_{c,max}$ | $f_{c,\overline{T}_{max},t_T}$ (MPa) | Confinement factor $\xi_{T_{max}}$ | Tests (kN) | Predicted (kN) |
|---|---|---|---|---|---|---|---|
| S0CA0-T1-219 | 955 | 354 | 656 | 63 | 0.32 | 3191 | 3146 |
| S2CA0-T1-219 | 960 | 353 | 713 | 57 | 0.356 | 2952 | 3225 |
| S2CA15-T1-219 | 963 | 352 | 726 | 64 | 0.312 | 3229 | 3680 |
| S2CA30-T1-219 | 965 | 351 | 730 | 68 | 0.297 | 3339 | 3754 |
| S0CA0-T2-219 | 858 | 385 | 560 | 86 | 0.257 | 4074 | 3683 |
| S2CA0-T2-219 | 860 | 385 | 574 | 95 | 0.231 | 4402 | 4410 |
| S2CA15-T2-219 | 866 | 383 | 605 | 106 | 0.207 | 4776 | 4662 |
| S2CA30-T2-219 | 870 | 381 | 615 | 110 | 0.199 | 4916 | 5069 |

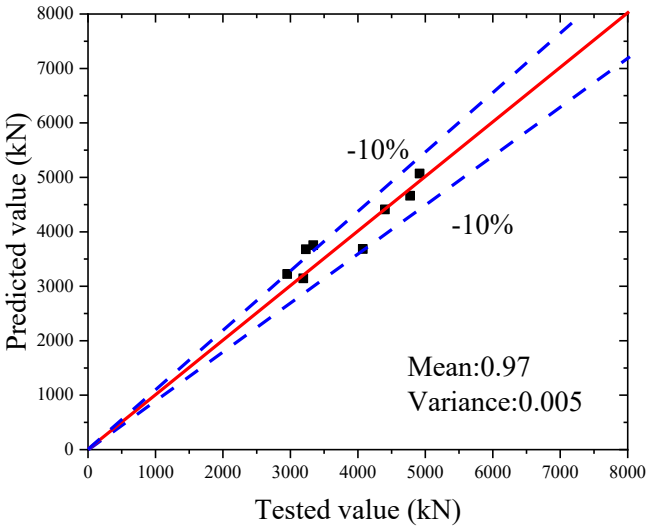


Figure 19 The validation of the proposed method

From the structure and formulation of the method, it can be observed that, although the proposed bearing capacity calculation method is specifically designed for UHPCFST, the model exhibits strong compatibility and can be extended to predict the post-fire residual strength of normal CFST stub columns by adjusting the average historical maximum temperature and the equivalent strength of the core concrete.

## 5 Conclusion

The paper presents the experimental investigation on 27 UHPCFST stub columns under axial compression after being exposed to elevated temperatures at early age. The failure modes, cross-sectional historical-max temperatures, axial load-deformation curves, and residual compression of the specimens are analysed. Based on the present study, the following conclusions are drawn:

1）For columns exposed to fire sources at greater distances (T1), diagonal shear failure was observed from all the specimens. When exposed to nearby fire sources (T2), bulging was the main failure mode.

2）The historical-max temperatures of both the steel tube and the core UHPC increase with UHPC age. Furthermore, with an increased proportion of coarse aggregate, the historical-max temperatures of both the steel tube and the UHPC gradually rise across different ages.

3）For columns exposed to fire sources at greater distances (T1), there is a notable enhancement in the bearing capacity after high-temperature exposure and subsequent curing at different ages. The capacity shows an increasing trend with the growth of the UHPC age exposed to high-temperature. When exposed to nearby fire sources (T2), a reduction in strength is observed, and the overall bearing capacity

of the column exhibits a decreasing trend with the growth of the UHPC age exposed to high-temperature.

4）For columns exposed to fire sources at greater distances (T1), their stiffness is slightly reduced in comparison to components matured at ambient temperature, with relative stiffness ranging between 0.85 and 0.95. Furthermore, the overall stiffness of the columns exhibits an increasing trend with the duration of high-temperature aging. Similarly, as exposed to nearby fire sources (T2), their stiffness experiences a more noticeable reduction compared to the components matured at ambient temperature, with relative stiffness ranging between 0.55 and 0.65. Moreover, the overall stiffness of the columns demonstrates a decreasing trend with the duration of high-temperature aging, a trend mitigated with the addition of aggregate.

**Acknowledge**

This study was supported financially by the National Natural Science Foundation of China (Grant NO. 52178157).

**Reference**

[1] Shi C, Wu Z, Xiao J, Wang D, Huang Z, Fang Z. A review on ultra high performance concrete: Part I. Raw materials and mixture design. Constr Build Mater. 2015;101741-51.

[2] Ye M, Li L, Pei B, Yoo D, Li H, Zhou C. A critical review on shear performance of joints in precast Ultra-High-Performance Concrete (UHPC) segmental bridges. Eng Struct. 2024;301117224.

[3] Li Y, Zhang D. Effect of lateral restraint and inclusion of polypropylene and steel fibers on spalling behavior, pore pressure, and thermal stress in ultra-high-performance concrete (UHPC) at elevated temperature. Constr Build Mater. 2021;271121879.

[4] Lyu X, Ahmed T, Elchalakani M, Yang B, Youssf O. Influence of crumbed rubber inclusion on spalling, microstructure, and mechanical behaviour of UHPC exposed to elevated temperatures. Constr Build Mater. 2023;403133174.

[5] Chen Z, Wang X, Ding L, Jiang K, Liu X, Liu J, et al. Spalling resistance and mechanical properties of ultra-high performance concrete reinforced with multi-scale basalt fibers and hybrid fibers under elevated temperature. J Build Eng. 2023;77107435.

[6] Li Y, Pimienta P, Pinoteau N, Tan KH. Effect of aggregate size and inclusion of polypropylene and steel fibers on explosive spalling and pore pressure in ultra-high-performance concrete (UHPC) at elevated temperature. Cement Concrete Comp. 2019;9962-71.

[7] Deng F, Xu L, Chi Y, Wu F, Chen Q. Effect of steel-polypropylene hybrid fiber and coarse aggregate inclusion on the

stress–strain behavior of ultra-high performance concrete under uniaxial compression. Compos Struct. 2020;252112685.

[8] Xu L, Wu F, Chi Y, Cheng P, Zeng Y, Chen Q. Effects of coarse aggregate and steel fibre contents on mechanical properties of high performance concrete. Constr Build Mater. 2019;20697-110.

[9] Yang K, Long G, Tang Z, Li W, Ma G, Li C, et al. Enhancing the flexural toughness of UHPC through flexible layer-modified aggregates: A novel interfacial toughening strategy. Cement Concrete Comp. 2024;154105770.

[10] Jin L, Xie C, Yu W, Du X. Effect of steel fiber content on failure strength and toughness of UHPC-CA at low temperature: An experimental investigation. J Build Eng. 2024;94109976.

[11] Xue C, Yu M, Wu M, Cheng S. Axial compressive behaviour of ultra-high performance concrete filled steel tube stub columns at elevated temperatures. Structures. 2023;57105333.

[12] Wu F, Xu L, Zeng Y, Yu M, Li B. Behavior of CA-UHPC filled circular steel tube stub columns under axial compression. J Constr Steel Res. 2023;211108204.

[13] Yu M, Liao W, Liu S, Wang T, Yu C, Cheng S. Axial compressive performance of ultra-high performance concrete-filled steel tube stub columns at different concrete age. Structures. 2023;55664-76.

[14] Cai H, Xu L, Chi Y, Yan Y, Yu C, He C. Seismic performance of rectangular ultra-high performance concrete filled steel tube (UHPCFST) columns. Compos Struct. 2021;259113242.

[15] Yu C, Yu M, Xu L, Liu S, Wang T, Ye J. Experimental research on mechanical behavior of UHPCFST under repeated axial compression. J Constr Steel Res. 2024;218108690.

[16] Xiong M, Liew JYR. Buckling behavior of circular steel tubes infilled with C170/185 ultra-high-strength concrete under fire. Eng Struct. 2020;212110523.

[17] Yao T, Ma K, Xing G, Qiao L. Axial compression performance of UHPCFCST stub columns after exposure to high temperatures. J Constr Steel Res. 2023;210108092.

[18] Wang T, Yu M, Zhang X, Jianqiao Y. Experimental Study on Random Temperature Field of Ultra-High Performance Concrete Filled Steel Tube Columns under Elevated Temperature. Compos Struct. 2022;289115445.

[19] Wang T, Yu M, Zhang X, Xu L, Huang L. Experimental study and proposal of a design model of ultra-high performance concrete filled steel tube columns subjected to fire. Eng Struct. 2023;280115697.

[20] Wang T, Yu M, Zhang X, Cheng S, Liu S. Post-fire mechanical behaviour of ultra-high-performance concrete-filled steel tube (UHPCFST) stub columns under compression. J Constr Steel Res. 2022;196107384.

[21] Jin W, Song Z, Zhao Y. Life-cycle reliability of engineering structures and structure safety under hazard events. Journal

Of Zhejiang University(Engineering Science). 2006;401862-8.

[22] Mendez A. Some evacuees cleared to return home after 8-alarm Redwood City fire. 2024. https://www.nbcbayarea.com/news/local/peninsula/redwood-city-fire-prompts-evacuations/3555630/?os=nirstv&ref=app.

[23] Quan'Er C. Sudden! A fire broke out on a construction project in the urban area of Chengde, with thick smoke billowing at the scene. 2020. https://www.163.com/dy/article/FRD6HVHD0545QOQP.html.

[24] Wikipedia. Notre-Dame fire. 2019. https://en.wikipedia.org/wiki/Notre-Dame_fire.

[25] R C. Fires in structures under construction or renovation.: National Fire Protection Association(NFPA), 2020.

[26] Xu S, Wang H, Zeng Q, Liu J, Qu H. Structural assessment and treatment of post-fire building under construction. Building Structure. 2018;4818-23.

[27] Guodong, Huang G, Zhang R, Zhang R, Li H,Guo H. The influence of high temperature on the mechanical properties of early age concrete. Railway Engineering. 2019;593.

[28] ISO 834-13:2019. Fire-resistance tests — Elements of building construction — Part 2: Requirements and recommendations for measuring furnace exposure on test samples. Standardization International Organization, 2019.

[29] ASTM E119-24. Standard test methods for fire tests of building construction and materials. US-ANSI, 2000.

[30] CN-GB. Fire resistance test for elements of building construction—Alternative and additional procedures. GB/T 26784-2011: Standards Press of China, 2011.

[31] Wei J. Numerical simulation analysis of fire in multi-storey building under construction. Xian University of Architecture and Technolo; 2017.

[32] Zhou B, Zhang T, Xu Y. Application of numerical simulation technology in the analysis of constructing high-rise fires. Journal of Institute of Disaster-prevention science And Technology. 2008;1028-32, 49.

[33] Yang Y, Wu L. Research on the influence factors on the fire smoke movement in building under construction. Fire Science and Technology. 201646-9.

[34] Hou X, Ren P, Rong Q, Zheng W, Zhan Y. Comparative fire behavior of reinforced RPC and NSC simply supported beams. Eng Struct. 2019;185122-40.

[35] ASTM. Standard test method for slump flow of self-consolidating concrete. ASTM C1611/C1611M2018.

[36] GB/T 228.1-2010. Matallic materials — tensile testing — Part 1： method of test at room temperature. Standardization Administration of the People's Republic of China, 2010.

[37] Lin J Zhang Y, Guo Z, et al. Impact of synthetic fibers on spalling and intrinsic pore structure of ultra-high

performance concrete (UHPC) under elevated temperatures. Constr Build Mater. 2024,439137325.

[38] Zhang Y, Zhang S, Zhao W, et al. Spalling behavior in ultra-high performance concrete: multi-technique insights and multi-scale fiber-rubber mitigation strategies. J Build Eng. 2024,98111333.

[39] Feng P, Cheng S, Bai Y, Ye L. Mechanical behavior of concrete-filled square steel tube with FRP-confined concrete core subjected to axial compression. Compos Struct. 2015;123312-24.

[40] Peng G, Niu X, Shang Y, Zhang D, Chen X, Ding H. Combined curing as a novel approach to improve resistance of ultra-high performance concrete to explosive spalling under high temperature and its mechanical properties. Cement Concrete Res. 2018;109147-58.

[41] Zheng W, Li H, Wang Y. Compressive behaviour of hybrid fiber-reinforced reactive powder concrete after high temperature. Mater Design. 2012;41403-9.

[42] Huo J, Huang G, Yan X. Effects of sustained axial load and cooling phase on post-fire behaviour of concrete-filled steel tubular stub columns. J Constr Steel Res. 2009;651664-76.

[43] Yang H, Han L. Practical calculation method for residual load bearing capacities of concrete-filled steel tubular columns with rectangular cross-sections after exposure to the ISO-834 standard fire. Annual Meeting of China Steel Construction Society Association for Steel-Concrete Composte Structures2005.

[44] Jiang S, Yu Q, Li Y. Calculation method of bearing capacity of rectangular concrete-filled steel tubular members after high temperature subjected to biaxial force and bending. Journal of Shenyang Jianzhu University(Natural science). 2009;025495-500.

[45] Li Y, Wang Z. Research on Residual Loading Capacity of Concrete－filled Square Steel Tube Stub Columns After Exposure to Fire. Journal of Water Resources and Architectural Engineering. 2015;1379-84.

[46] Lv X. Residual load capacity and experimental research on short steel tube infilled with high strength concrete columnn Post-Fire .Nanjing,Southeast University,2018.

[45] Shi G, Wang S, Rong C. Experimental investigation into mechanical properties of Q345 steel after fire. J Constr Steel Res. 2022;199107582.

[47] Jie T. Study on the mechanical properties of ultra-high performance concrete under compression at early age after exposure to normal and elevated temperature.Wuhan,Wuhan University, 2023.